THE JOURNAL OF BIOLOGICAL CHEMISTRY VOL. 285, NO. 2, pp. 1283–1295, January 8, 2010

Ionizing Radiation Induces Cellular Senescence of Articular Chondrocytes via Negative Regulation of SIRT1 by p38 Kinase*

Received for publication, August 21, 2009, and in revised form, October 14, 2009 Published, JBC Papers in Press, November 2, 2009, DOI 10.1074/jbc.M109.058628

Eun-Hee Hong[‡], Su-Jae Lee[§], Jae-Sung Kim[‡], Kee-Ho Lee[‡], Hong-Duck Um[‡], Jae-Hong Kim[¶], Song-Ja Kim[‖], Jong-Il Kim[**], and Sang-Gu Hwang[‡1]

*From the [‡]Division of Radiation Cancer Research, Korea Institute of Radiological and Medical Sciences, Seoul 139-706, the [§]Department of Chemistry, College of Natural Sciences, Hanyang University, Seoul 133-791, the [¶]Graduate School of Biotechnology, Korea University, Seoul 136-701, the [‖]Department of Biological Sciences, College of Natural Sciences, Kongju National University, Gongju 314-701, and the **Department of Food and Microbial Technology, College of Natural Sciences, Seoul Women's University, Seoul 139-774, Korea*

Radiotherapy is increasingly used in the treatment of joint diseases, but limited information is available on the effects of radiation on cartilage. Here, we characterize the molecular mechanisms leading to cellular senescence in irradiated primary cultured articular chondrocytes. Ionizing radiation (IR) causes activation of ERK, in turn generating intracellular reactive oxygen species (ROS) with induction of senescence-associated β-galactosidase (SA-β-gal) activity. ROS activate p38 kinase, which further promotes ROS generation, forming a positive feedback loop to sustain ROS-p38 kinase signaling. The ROS inhibitors, nordihydroguaiaretic acid and GSH, suppress phosphorylation of p38 and cell numbers positive for SA-β-gal following irradiation. Moreover, inhibition of the ERK and p38 kinase pathways leads to blockage of IR-induced SA-β-gal activity via reduction of ROS generation. Although JNK is activated by ROS, this pathway is not associated with cellular senescence of chondrocytes. Interestingly, IR triggers down-regulation of SIRT1 protein expression but not the transcript level, indicative of post-transcriptional cleavage of the protein. SIRT1 degradation is markedly blocked by SB203589 or MG132 after IR treatment, suggesting that cleavage occurs as a result of binding with p38 kinase, followed by processing via the 26 S proteasomal degradation pathway. Overexpression or activation of SIRT1 significantly reduces the IR-induced senescence phenotype, whereas inhibition of SIRT1 activity induces senescence. Based on these findings, we propose that IR induces cellular senescence of articular chondrocytes by negative post-translational regulation of SIRT1 via ROS-dependent p38 kinase activation.

Radiotherapy, a curative medical intervention, involves the use of high energy x-rays or γ-rays and is integral to the multidisciplinary approach to treat patients with musculoskeletal neoplasms. Advances in radiotherapy and its delivery have made feasible unexpected applications in bone tumors, such as Ewing's sarcoma and osteosarcoma, as well as soft tissue sarcomas, such as chondrosarcoma and synovial sarcoma (1, 2). Higher doses are associated with side effects during the course of radiotherapy, whereas low dose palliative treatments cause minimal or no side effects. For example, the application of radiotherapy in skeletally immature patients frequently results in asymmetric limb growth arrest, angular deformities, and resultant limb length discrepancy (3–5). Sprague-Dawley rats display markedly inhibited proliferation in the proximal tibia growth plate after irradiation. This inhibition results from the coordination of a number of genes related to growth factors and cytokines and sequential responses to irradiation (6). Several reports have focused on the mechanisms underlying the inhibitory effects of radiotherapy on chondrocyte proliferation and differentiation (7, 8). However, the signal transduction mechanisms of irradiation-induced cellular senescence of joint tissue cartilage are yet to be fully established.

Senescent cells commonly exhibit irreversible growth arrest, large flat morphology, and up-regulated senescence-associated β-galactosidase (SA-β-gal)[2] activity at pH 6.0 (9, 10). Several conditions, including oncogenic stress, oxidative stress, and DNA damage, are associated with cellular senescence. Activated *ras* and *raf* oncogenes in NHF cells induce rapid onset of senescence independent of telomerase (11, 12). Reactive oxygen species (ROS) promote telomere instability and dysfunction in chondrocytes, subsequently resulting in cartilage aging (13). Massive acute DNA double strand breaks occurring as a result of mechanical and chemical stress can be repaired, but some DNA damage persists, eventually triggering premature senescence (14, 15). Because ionizing radiation (IR) directly induces double strand break (16), it is possible that cellular senescence is activated under these conditions. Indeed, IR reportedly promotes a low or high frequency senescence-like phenotype in cultured plateau phase vascular endothelial cells (17, 18). Cellular senescence is additionally associated with a reduction in the regenerative capacity of tissue and represents a

* This work was supported by the Korea Research Foundation Grant KRF-2005-041-C00344 and a Nuclear Research and Development Program of the Korea Science and Engineering Foundation grant funded by the Korean Government.

[1] To whom correspondence should be addressed: Korea Institute of Radiological and Medical Sciences, 215-4 Gongneung-Dong, Nowon-Ku, Seoul 139-706, Korea. Tel.: 82-2-970-1353; Fax: 82-2-970-2417; E-mail: sgh63@kcch.re.kr.

[2] The abbreviations used are: SA-β-gal, senescence-associated β-galactosidase; ERK, extracellular signal-regulated kinase; IR, ionizing radiation; JNK, c-Jun N-terminal protein kinase; MAPK, mitogen-activated protein kinase; NDGA, nordihydroguaiaretic acid; OA, osteoarthritis; ROS, reactive oxygen species; Gy, grays; ALLnL, *N*-acetyl-leucyl-norleucinal; Z, benzyloxycarbonyl; MG132, Z-Leu-Leu-Leu-aldehyde; fmk, fluoromethylketone; PBS, phosphate-buffered saline; FRET, fluorescence resonance energy transfer; GFP, green fluorescent protein; RFP, red fluorescent protein; GST, glutathione *S*-transferase.

permanent form of cell cycle arrest in primary cultures. In view of these observations, one plausible theory is that chondrocyte senescence plays a pivotal role in the pathogenesis and development of osteoarthritis (OA). A recent series of studies provide strong and direct insights into this senescence-cartilage degeneration association (13, 19). However, the mechanical and biological events in articular chondrocytes following irradiation are poorly understood, and limited information is available on the molecular signal transduction mechanisms of cellular senescence at present.

The p38 mitogen-activated protein kinase (MAPK) pathway is activated under conditions of cellular stress, including ROS, UV light, x-ray, and inflammatory cytokines. Moreover, the roles of p38 kinase signaling in individual responses are diverse, depending on the cell type and stimulus (20, 21). Several reports suggest that the p38 pathway is associated with cellular senescence. Oncogenic Ras indirectly activates p38 kinase, which is involved in Ras-ERK MAPK-induced senescence in primary human and murine fibroblast lines (22). The Bcl-2 family protein Bcl-xL inhibits p53-induced senescence by preventing ROS-dependent p38 activation in EJ human bladder carcinoma cells (23). Constitutive activation of p38 kinase promotes cell cycle arrest, which becomes permanent and irreversible, in association with the biochemical features of senescence in human osteoblast-like cancer cells (24, 25). In addition, p38 kinase activation in response to IR appears variable (*i.e.* either weak (26) or strong via the functional ATM protein (27, 28)). These findings indicate that p38 plays a causative role in several types of senescence programs and further support the possibility of IR involvement in cellular senescence. Based on the available data, we propose that exposure of cells to IR induces simultaneous compensatory activation of multiple MAPK pathways. However, the ERK and JNK pathways appear to be in a dynamic balance in response to IR, with the prosurvival ERK pathway acting to inhibit the proapoptotic JNK pathway. To date, $p16^{INK4A}$ and p53 have been identified as two major effectors of p38 kinase in the regulation of senescence phenotypes (29). It is important to further determine the p38 kinase downstream signaling events mediating cellular senescence.

In this study, we identify SIRT1, a mammalian Sir2 ortholog, as a target molecule of p38 kinase that acts in regulating cellular senescence of articular chondrocytes. SIRT1, a nicotine adenine dinucleotide (NAD)-dependent deacetylase, modulates a diverse set of pathways implicated in the aging process (30). The protein is additionally involved in a number of cellular processes, including transcriptional silencing, DNA damage, recombination, cell division cycles, and chromosomal stability. To perform these functions, SIRT1 interacts physically with and regulates histone proteins (31) and diverse important nuclear substrates, including the tumor suppressor p53 (32, 33), forkhead transcription factor (FOXO) (34, 35), the RelA/p65 subunit of NF-κB (36), peroxisome proliferator-activated receptor-γ (37), and DNA repair factors E2F1 (38) and Ku70 (39). Although it is established that SIRT1 promotes or inhibits cellular senescence under conditions of DNA damage, oxidative stress, and dietary restriction, the underlying regulatory mechanisms remain unclear. Here, we demonstrate that the interactions between p38 kinase and SIRT1 protein play an important role in the regulation of cellular senescence in response to IR.

EXPERIMENTAL PROCEDURES

Primary Culture of Rabbit Articular Chondrocytes—Individual articular chondrocytes were isolated from joint cartilage slices of 2-week-old New Zealand White rabbits by enzymatic digestion. Briefly, after aseptic dissection, cartilage slices were dissociated enzymatically for 4 h in 0.2% collagenase type II (381 units/mg solid; Sigma) in Dulbecco's modified Eagle's medium (Invitrogen). Single cells were obtained by collecting the supernatant after brief centrifugation and resuspended in Dulbecco's modified Eagle's medium supplemented with 10% (v/v) fetal bovine serum, 50 μg/ml streptomycin, and 50 units/ml penicillin (Invitrogen). Cells were plated on culture dishes at a density of 5×10^4 cells/cm^2. The medium was changed every 1.5 days after seeding, and cells reached confluence after ~5 days. Chondrocytes were cultured as monolayers in a humidified atmosphere of 5% CO_2 in air.

Treatment of Cells—Cells were irradiated using a ^{137}Cs-ray source (Atomic Energy of Canada, Ltd., Mississauga, Canada) at a dose rate of 3.81 Gy/min. In all experiments, IR was acute delivered within the first 2.6 min of culture and then followed by cell incubation for the specified time. For inhibitor or activator studies, the respective chemicals were added 1 h prior to radiation treatment. Nordihydroguaiaretic acid (NDGA) and GSH (Sigma) were used to scavenge ROS. SB203580, PD98059, and SP600125 to inhibit p38, ERK, and JNK were used (Calbiochem), respectively. The proteasome inhibitors, Z-Leu-Leu-Leu-aldehyde (MG132) and *N*-acetyl-leucyl-norleucinal (ALLnL), and the calpain inhibitor, *N*-acetyl-leucyl-leucyl-methioninal, were acquired from Sigma. The peptide caspase inhibitors, benzyloxycarbonyl-Val-Ala-Asp-fluoromethylketone (Z-VAD-fmk) and benzyloxycarbonyl-Asp-Glu-Val-Asp-fluoromethylketone (Z-DEVD-fmk), were obtained from Biomol Research Laboratory Inc. (Plymouth Meeting, PA). We employed resveratrol to activate SIRT1 and nicotinamide to inhibit SIRT1 (Sigma).

Cell Proliferation and Morphology—Chondrocytes were plated on culture dishes at a density of 5×10^4 cells/cm^2. Cells were treated with IR according to the designated experimental conditions in the absence or presence of the indicated pharmacological reagents. Cell proliferation was determined by direct counting using a hemocytometer, and alterations in cellular morphology were observed by microscopy.

SA-β-gal Staining and Quantification—Detection of SA-β-gal activity at pH 6 was performed essentially as described by Dimri *et al.* (10). Briefly, IR-treated or untreated chondrocytes were cultured under the designated experimental conditions. Cells were washed twice with phosphate-buffered saline (PBS) and fixed with 3.7% formaldehyde solution for 10 min. The fixer was removed by washing twice with PBS, and cells were incubated at 37 °C with SA-β-gal staining solution (1 mg/ml of 5-bromo-4-chloro-3-indolyl β-D-galactoside (Promega), 40 mM citric acid/sodium phosphate buffer, pH 6.0, 5 mM potassium ferrocyanide, 5 mM potassium ferricyanide, 150 mM NaCl, 2 mM $MgCl_2$). Staining was evaluated after a 16-h incubation at oven temperature in a CO_2-free atmosphere. The percentages

of SA-β-gal-positive cells were determined by scoring ~200 cells/sample.

Assay for ROS—Chondrocytes were treated with IR according to the experimental conditions in the absence or presence of ROS or MAPK inhibitors. Cells were incubated with 10 nM DCF-DA (Molecular Probes, Inc., Eugene, OR) in the dark at 37 °C for 30 min to detect ROS. Initially, cells were harvested by trypsinization, washed three times with PBS, and subjected to measurement on a FACScan flow cytometer. ROS levels are expressed as a histogram of the fluorescence generated by 10,000 cells. Subsequently, cell staining was examined with a laser-scanning confocal microscope (model LSM 710, Carl Zeiss) equipped with an argon laser tuned to an excitation wavelength of 488 nm, LP505 emission filter (515–540 nm), and Zeiss Axiovert ×100 objective lens. Four groups of cells were randomly selected from each sample.

Reverse Transcription-PCR—Chondrocytes were treated with IR, as specified in each experiment. Total RNA was isolated using RNA STAT-60 (Tel-Test B, Friendswood, TX). Reverse transcription reactions were performed using ImProm-II (Promega) with rTaq polymerase (TaKaRa Bio Inc., Shiga, Japan) for 5 min at 70 °C for annealing and 60 min at 42 °C for extension of the first strand. The following primers and conditions were employed: type II collagen (*COL2A1*) (370-bp product, annealing temperature 60 °C, 20 cycles), sense (5′-GAC CCC ATG CAG TAC ATG CG-3′) and antisense (5′-AGC CGC CAT TGA TGG TCT CC-3′); Sox-9 (386-bp product, annealing temperature 62 °C, 27 cycles), sense (5′-GCG CGT GCA GCA CAA GAA GGA CCA CCC GGA TTA CAA GTA C-3′) and antisense (5′-CGA AGG TCT CGA TGT TGG AGA TGA CGT CGC TGC TCA GCT C-3′); glyceraldehyde-3-phosphate dehydrogenase (299-bp product, annealing temperature 50 °C, 21 cycles), sense (5′-TCA CCA TCT TCC AGG AGC GA-3′) and antisense (5′-CAC AAT GCC GAA GTG GTC GT-3′); SIRT1 (586-bp product, annealing temperature 61 °C, 30 cycles), sense (5′-TAG AGA ACC TTT GCC TCA TC-3′) and antisense (5′-AAA ATG TAA CGA TTT GGT GG-3′); β-catenin (518-bp product, annealing temperature 52 °C, 27 cycles), sense (5′-GAA AAT CCA GCG TGG ACA ATG GCT ACT C-3′) and antisense (5′-ACC ATA ACT GCA GCC TTA TTA ACC-3′). The primers were designed based on the sequences of human Sox-9, SIRT1, and β-catenin genes. Sequencing of the resulting PCR products for rabbit Sox-9, SIRT1, and β-catenin revealed that these gene fragments were 93.0, 88.0, and 94.0% homologous to their human counterparts, respectively (data not shown). Quantitative real-time PCR was performed in triplicate using a chromo 4 cycler (Bio-Rad) and SYBR Premix Ex Taq™ (Takara Bio, Shiga, Japan). The amplification signal from the target gene was normalized against that of glyceraldehyde-3-phosphate dehydrogenase in the same reaction.

Reporter Gene Assay—NF-κB and Sox-9 activation were examined by analyzing the degradation of inhibitor protein κB (I-κB) and Sox-9 using Western blot analysis and directly with a reporter gene assay. For the reporter gene assay, chondrocytes were transfected with an NF-κB plasmid containing luciferase and three tandem repeats of serum response element, Sox-9 plasmid containing luciferase and the 48-bp Sox-9 binding site in the first intron of human *COL2A1*, or a control vector using Lipofectamine PLUS (Invitrogen), as described previously (40). Transfected cells were cultured in complete medium for 24 h, treated with 10 Gy of IR for the additional indicated times in each experiment, and used to determine luciferase activity with an assay kit from Promega. Luciferase activity was normalized against that of β-galactosidase.

Ectopic Expression of Wild-type or Dominant Negative p38 Kinase—Chondrocytes from day 2 cultures were transfected with pcDNA3.1 plasmids coding for wild-type or dominant-negative p38 kinase using Lipofectamine PLUS (Invitrogen), following the procedure recommended by the manufacturer. After incubation in complete medium for 24 h, transfected cells were treated with 10 Gy of IR for an additional 36 h.

Construction of Retrovirus and Infection—cDNA for wild-type SIRT1 or dominant-negative SIRT1 (SIRT1-HY) was subcloned into the retroviral vector, pMFG-puro (32, 33). H29D packaging cells were transiently transfected with pMFG-puro, MFG-SIRT1, or MFG-SIRT1-HY alone. The viral supernatant was collected, filtered, and supplemented with 8 μg/ml Polybrene. Chondrocytes from day 2 cultures were infected with either control retrovirus or retrovirus containing wild-type SIRT1 or mutant SIRT-HY cDNA for 4 h. After incubation of infected cells in complete medium for 24 h, cells were left untreated or treated with 10 Gy of IR for an additional 48 h.

Determination of Apoptosis—Chondrocytes were plated on 35-mm dishes at a cell density of 4×10^5 cells and subjected to various doses of IR for 48 h. For quantification of cell death, cells were trypsinized, washed in PBS, incubated in propidium iodide (2.5 mg/ml) for 5 min at room temperature, and analyzed with the FACScan flow cytometer. To determine the mitochondrial membrane potential ($\Delta\Psi_m$), cells were incubated in 30 nM 3,3′-dihexyloxacarboxyanine iodide (Molecular Probes, Inc.) at 37 °C for 30 min, harvested by trypsinization, and washed three times with PBS. $\Delta\Psi_m$ was additionally determined using a FACScan flow cytometer. For isolation of the cytosolic fraction, cells were lysed with lysis buffer (20 mM HEPES, pH 7.5, 250 mM sucrose, 10 mM KCl, 2 mM $MgCl_2$, 1 mM EDTA, 1 mM dithiothreitol, protease inhibitor mixture) for 20 min on ice. Samples were homogenized using a Dounce glass homogenizer with a loose pestle (Wheaton, Millville, NJ) for 70 strokes. The homogenate was centrifuged at 12,000 rpm for 20 min at 4 °C. Protein levels of cytochrome *c* and tubulin were analyzed by Western blot analysis. The formation of high molecular weight and oligonucleosomal DNA fragments was examined by agarose gel electrophoresis with an apoptotic DNA ladder isolation kit (Biovision Inc., Mountain View, CA).

Immunoprecipitation—Chondrocytes were washed twice with PBS, harvested, and lysed for 15 min in buffer (50 mM Tris-HCl (pH 7.4), 150 mM NaCl, and 0.1% Triton X-100) containing protease and phosphatase inhibitors, as described below. Samples were diluted to 500 μg of protein in 600 ml of buffer and precleared for 1 h at 4 °C with 40 μl of a 1:1 slurry of protein G-Sepharose beads (GE Healthcare). After brief centrifugation to remove precleared beads, 1 μg of antibody against p38 or SIRT1 was added to each sample and incubated on a rocking platform at 4 °C overnight. The immune complex was precipitated by incubating with 40 μl of protein G-Sepharose

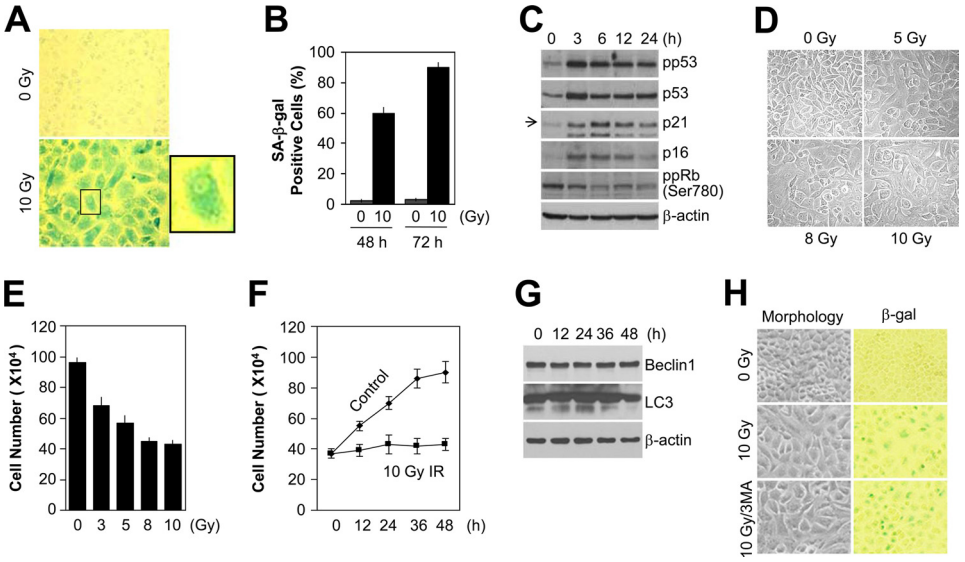

FIGURE 1. **IR induces cellular senescence of primary cultured articular chondrocytes.** *A* and *B*, chondrocytes were left untreated or treated with 10 Gy of IR and then incubated for 72 h (*A*) or 48–72 h (*B*). Cellular senescence was evaluated with the SA-β-gal assay. The photomicrographs depict SA-β-gal-positive cells (*blue*, *A*). The *graph* represents the percentages of SA-β-gal positive cells counted manually from a total of 200 cells (*B*). *C*, chondrocytes were treated with 10 Gy of IR and incubated for the indicated periods. Protein levels of p53, p21, and p16 and phosphorylation levels of p53 and pRb were detected by Western blotting. β-Actin was used as the loading control. *D* and *E*, chondrocytes were treated with the specified concentrations of IR and followed by a 48-h incubation. Cell morphology was observed using light microscopy (*D*), and the total cell number was quantified by counting the surviving cells using trypan blue solution (*E*). *F* and *G*, chondrocytes were treated with 10 Gy of IR and incubated for the indicated periods. The total cell number was quantified by counting the surviving cells using trypan blue solution (*F*), and protein levels of beclin1 and LC3 were detected by Western blotting (*G*). β-Actin was used as the loading control. *H*, chondrocytes were left untreated or treated with 10 Gy of IR in the absence or presence of 10 μM 3-methyladenine (*3MA*) and then incubated for 48 h. Cell morphology was observed using light microscopy (*left*), and cellular senescence was evaluated with the SA-β-gal assay (*right*). The photomicrographs depict SA-β-gal-positive cells (*blue*, *right*). Data are presented as results of a representative photomicrograph (*A*, *D*, and *H*), mean values with S.D. (*B*, *E*, and *F*), or a typical experiment (*C* and *G*) from at least four independent experiments.

beads at 4 °C for 2 h. Beads were washed five times with immunoprecipitation buffer. Half of the immunoprecipitated sample was assessed to confirm immunoprecipitation, and associated SIRT1 or p38 was examined in the second half of the samples via Western blot analysis.

GST Pull-down Assay—GST or GST-p38 fusion protein (1 μg) was incubated for 4 h on a rotator in a cold room with 1 mg of total cell lysate prepared in Nonidet P-40 buffer (50 mM Tris, pH 8.0, 150 mM NaCl, 1% Nonidet P-40). GST or GST-p38 kinase complexes were collected using GST-beads (Sigma) and washed three times with Nonidet P-40 buffer. The bound proteins were size-fractionated by electrophoresis and detected using Western blotting.

Fluorescence Resonance Energy Transfer (FRET) Analysis—Human SIRT1 (NM_012238-isotype A; 2244 bp) was amplified by PCR with NheI and BamHI sites added to the 5′- and 3′-ends, respectively. The primers used were 5′-GCCGCTAGCGGCCACCATGGCGGACGAGGCGGCCCTC-3′ (forward) and 5′-CGGGATCCCGTGATTTGTTTGATGGATAGTT-3′ (reverse). The PCR product was cloned into the pAcGFP vector (Clontech). Human p38 (NM_001315, 1083 bp) was amplified by PCR with XhoI and KpnI sites added to the 5′- and 3′-ends, respectively. The used primers are 5′-CCCTCGAGGGGCCACCATGTCTCAGGAGAGGCCCACG-3 (forward) and 5′-CGGGGTACCCCGGGACTCCATCTCTTCTTGGTC-3 (reverse). The PCR product was cloned into pDsRed-Monomer-Hyg-C1 vector (Clontech). All constructs were confirmed by DNA sequencing. For confocal microscopy, chondrocytes (4×10^5 cells/35-mm dish) were plated on coverslips and cotransfected with SIRT1-GFP and p38-RFP plasmid DNA using Lipofectamine PLUS (Invitrogen). After 48 h, transfected cells were imaged using a Zeiss LSM 510Meta confocal imaging system with a 30-milliwatt argon laser and a ×63 1.4 numerical aperture oil immersion objective. To measure FRET signals by acceptor photobleaching, a prebleached SIRT1-GFP image was collected, and the fluorescent intensity in a selected region of interest was recorded using the software provided by the manufacturer. p38-RFP fluorescence was then photodestroyed by repeated scanning with the 568-nm laser line. A second postbleach image of SIRT1-GFP in the same region of interest was collected. The fluorescent intensities of the two SIRT1-GFP images (pre- and postbleached) were compared. Colocalization of non-fused GFP and RFP were similarly processed. FRET was measured as an increase in GFP fluorescence intensity following RFP photobleaching. FRET efficiency was calculated as 100 × ((GFP postbleach − GFP prebleach)/GFP postbleach) using the FRET Macro in the Zeiss Aim software package, taking into account GFP and RFP background noise in each channel.

Western Blot Analysis—Chondrocytes were lysed in buffer containing 50 mM Tris-HCl (pH 7.5), 150 mM NaCl, 0.5% Nonidet P-40, and 0.1% SDS supplemented with protease inhibitors (10 μg/ml leupeptin, 10 μg/ml pepstatin A, 10 μg/ml aprotinin, and 1 mM 4-(2-aminoethyl) benzenesulfonyl fluoride) and phosphatase inhibitors (1 mM NaF and 1 mM Na_3VO_4). Proteins were fractionated by SDS-PAGE and transferred to a nitrocellulose membrane. Membranes were blocked with 5% nonfat dry milk in Tris-buffered saline and incubated with primary antibodies for 1 h at room temperature. The following antibodies were employed for detection: mouse monoclonal anti-ERK and -β-catenin (BD Transduction Laboratories); mouse monoclonal anti-p21 (BD PharMingen); rabbit polyclonal anti-cytochrome *c* (BD PharMingen); rabbit polyclonal anti-p38, -phospho-p38, -JNK, -phospho-JNK, -phospho-p53, -cleaved caspase-3, and -poly(ADP-ribose) polymerase (Cell Signaling Technology, Inc., Beverly, MA); rabbit polyclonal anti-acetyl-histone H3 (Millipore, Temecula, CA); mouse monoclonal anti-type II collagen (Chemicon, Temecula, CA); mouse monoclonal anti-β-actin (Sigma); rabbit polyclonal anti-ubiquitin (Sigma); mouse monoclonal anti-phospho-ERK, -p53, and

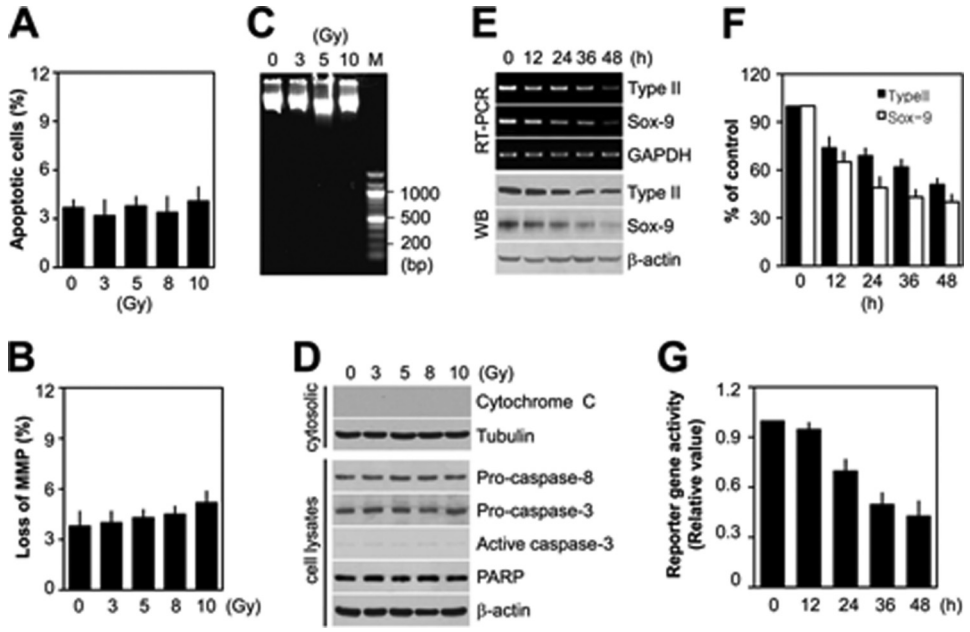

FIGURE 2. **IR does not induce cell death but promotes loss of type II collagen at high doses in primary cultured articular chondrocytes.** *A–D*, chondrocytes were treated with the specified concentrations of IR and followed by a 48-h incubation. Cell viability and mitochondrial membrane potential (*MMP*) were determined with the FACScan flow cytometer. Data are presented as the percentage of PI-positive cells (*A*) and loss of MMP (*B*), respectively. DNA samples were prepared and electrophoresed for DNA fragmentation analysis (*C*). The protein levels of cytochrome *c* and α-tubulin in cytosolic and caspase-8, caspase-3, active caspase-3, poly(ADP-ribose) polymerase (*PARP*), and β-actin in total cell lysates were detected by Western blotting (*D*). *E* and *F*, chondrocytes were treated with 10 Gy of IR and incubated for the indicated periods. Transcript levels of *COL2A1* and Sox-9 were determined by conventional PCR (reverse transcription-PCR; *RT-PCR*) (*E*, *top*) and quantitative real-time PCR (*F*), and protein levels of type II collagen, Sox-9, and β-actin were determined by Western blotting (*WB*) (*E*, *bottom*). Glyceraldehyde-3-phosphate dehydrogenase was used as the loading control or internal control. *G*, chondrocytes were transfected with the Sox-9 reporter gene for 24 h. Cells were then treated with 10 Gy of IR and incubated for the indicated periods. The transcriptional activity of Sox-9 was determined with the reporter gene assay. Data are presented as results of a typical experiment (*C–E*) or mean values with S.D. (*A*, *B*, *F*, and *G*) from at least four independent experiments.

-α-tubulin (Santa Cruz Biotechnology Inc., Santa Cruz, CA); rabbit polyclonal anti-Sox-9, -SIRT1, -beclin, -caspase-3, -caspase-8, -I-κB, -p16, phosphorylated Rb at Ser-780, and -GST (Santa Cruz Biotechnology, Inc.); and rabbit polyclonal anti-LC3 (Abgent, San Diego, CA). For the detection of ubiquitin, membranes were sandwiched between several sheets of Whatman 3M paper and submerged in deionized water, and membrane-bound ubiquitin was heat-activated by autoclaving for 30 min. Blots were developed using a peroxidase-conjugated secondary antibody and the ECL system (Amersham Biosciences).

RESULTS

IR Induces Cellular Senescence of Primary Cultured Articular Chondrocytes with Loss of Phenotype but No Cell Death at High Doses—To determine whether IR affects senescence of primary cultured articular chondrocytes, we initially assayed SA-β-gal activity (10), a specific cytoplasmic marker for senescent cells, after treatment with 10 Gy of IR. The cytosol stained positive for senescent cells (*blue*) (Fig. 1*A*), and ~60 and 90% of cells displayed SA-β-gal activity at 48 and 72 h, respectively (Fig. 1*B*). We next examined the patterns of the p53-Rb signaling pathway, which are known to be a crucial mediator of cellular senescence. As shown in Fig. 1*C*, p53 accumulation and phosphorylation at Ser-15 peaked 3 h after IR, and p21 was activated by a p53-dependent pathway. IR treatment resulted in induction of p16, a positive regulator of pRb, and thus caused hypophosphorylation and activation of pRb. Consistent with SA-β-gal activity, characteristics of senescence, such as large and flat morphology, were identified in cells treated with IR in a dose-dependent manner (Fig. 1*D*). Various doses of IR ranging from 0 to 10 Gy additionally caused a decrease in number of chondrocytes in a concentration-dependent manner at 48 h after irradiation (Fig. 1*E*), and this phenomenon was also dependent upon the time after irradiation with 10 Gy (Fig. 1*F*). Nevertheless, chondrocytes did not show any of the biochemical change that is associated with autophagy in response to IR. Up to 48 h after irradiation with 10 Gy, the conversion of LC3-I to LC3-II, a hallmark of mammalian autophagy, was not induced, as detected by Western blots for LC3 (Fig. 1*G*). In addition, pretreatment of macroautophagy inhibitor 3-methyladenine did not block IR-induced SA-β-gal activity and morphological change (Fig. 1*H*). These results indicate that IR induces cellular senescence of articular chondrocytes without induction of autophagy.

Next, we aimed to establish whether the decrease in cell number induced by IR is due to either growth inhibition or cell death. Cells were acute treated with several concentrations of IR, and the apoptotic cell death assay was performed at 48 h after irradiation. As shown in Fig. 2, no increase in the apoptotic cell content (Fig. 2*A*), disruption of mitochondria membrane potential (Fig. 2*B*), or DNA fragmentation (Fig. 2*C*) was evident after irradiation. Moreover, IR did not promote release of cytochrome *c* to the cytosol, activation of caspase-3 or cleavage of poly(ADP-ribose) polymerase (*PARP*; Fig. 2*D*). These data clearly indicate that the decreased cell number of IR-treated chondrocytes is attributed to the reduced proliferative potential of cells rather than induction of apoptotic cell death.

We further examined the phenotype of articular chondrocytes following IR exposure. Cells treated with 10 Gy of IR displayed reduced transcript and protein expression of cartilage-specific type II collagen as well as Sox-9, a major transcription factor that regulates type II collagen (*COL2A1*), in a time-dependent manner after irradiation (Fig. 2, *E* and *F*). In the reporter gene assay, reduced Sox-9 transcriptional activity was observed in IR-treated cells, consistent with Western blot data (Fig. 2*G*). Thus, it appears that IR induces dedifferentiation of articular chondrocytes, one of the underlying causes of OA.

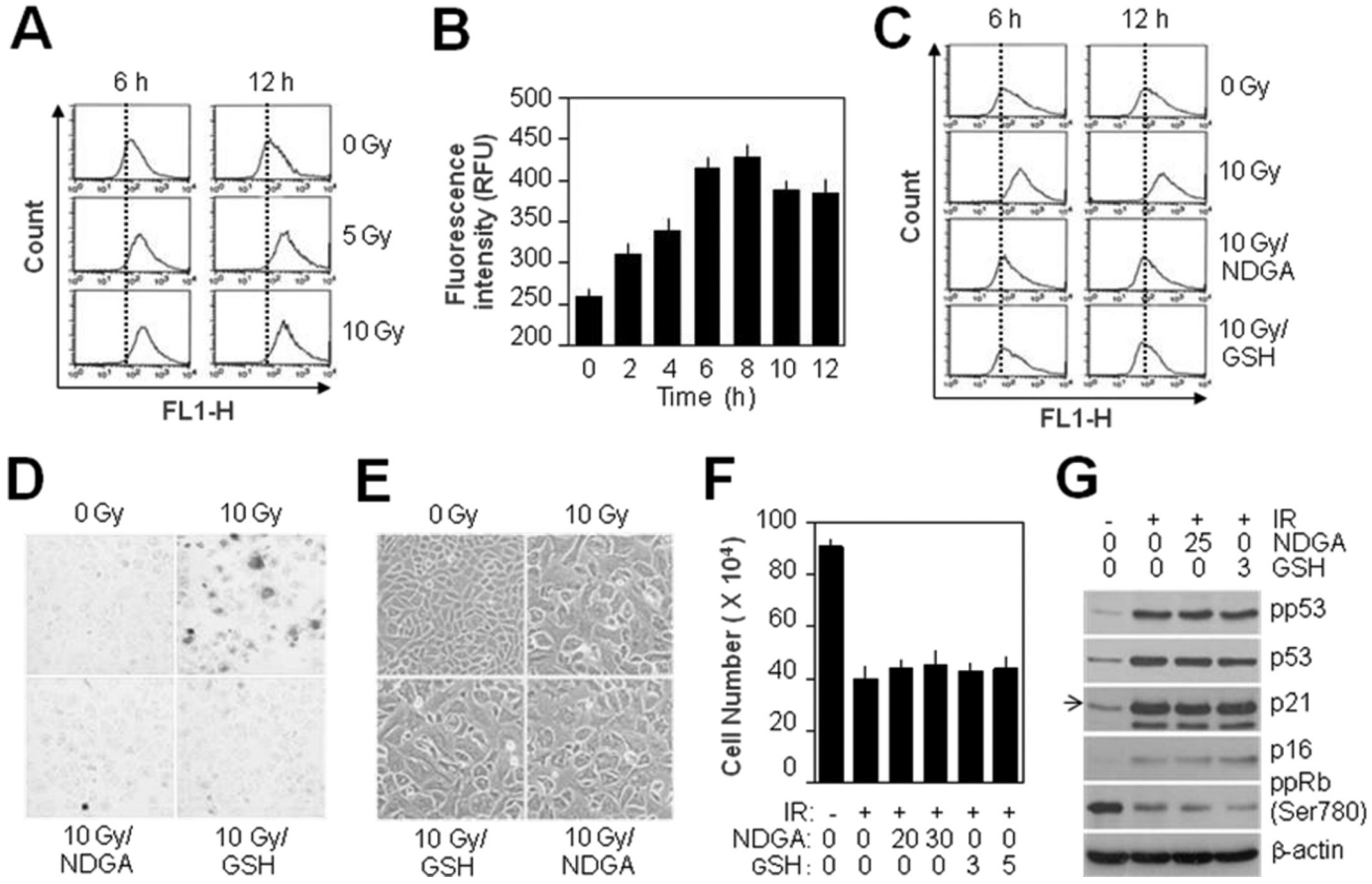

FIGURE 3. **IR-induced ROS is an important mediator of cellular senescence in primary cultured articular chondrocytes.** *A* and *B*, chondrocytes were treated with the specified concentrations of IR (*A*) or 10 Gy of IR (*B*) and then incubated for 6 and 12 h (*A*) or for the indicated periods (*B*). ROS production was assessed with the FACScan flow cytometer. *C–E*, chondrocytes were left untreated or treated with 10 Gy of IR in the absence or presence of 25 μM NDGA or 3 mM GSH and then incubated for 6 and 12 h (*C*) or 48 h (*D* and *E*). Changes in ROS generation were determined with the FACScan flow cytometer (*C*), cellular senescence was evaluated with the SA-β-gal assay (*D*), and cell morphology was observed using light microscopy (*E*). *F*, chondrocytes were left untreated (−) or treated (+) with 10 Gy of IR in the absence or presence of NDGA (20 or 30 μM) or GSH (3 or 5 mM). At 48 h after irradiation, the total cell number was quantified by counting surviving cells using trypan blue solution. *G*, chondrocytes were left untreated (−) or treated (+) with 10 Gy of IR in the absence or presence of 25 μM NDGA or 3 mM GSH and then incubated for 3 h (for phospho-p53 and p53 detection) or 6 h (for p21, p16, and phospho-pRb (*ppRb*) detection). Protein levels of p53, p21, and p16 and phosphorylation levels of p53 and pRb were detected by Western blotting. β-Actin was used as the loading control. Data are presented as results of a typical experiment (*A*, *C*, and *G*), a representative photomicrograph (*D* and *E*), or mean values with S.D. (*B* and *F*) from at least four independent experiments.

ROS and Activated ERK and p38 MAPKs but Not JNK Are Important Mediators of IR-induced Cellular Senescence in Primary Cultured Articular Chondrocytes—Irradiation stimulates ROS production in various mouse bone marrow or human Hep G2 cells, measured in experiments using fluorescent dyes (41, 42). Consistent with these findings, at 6 and 12 h after irradiation, ROS levels increased significantly with the radiation dose in primary cultured articular chondrocytes (Fig. 3*A*). ROS production was continuously accumulated up to 8 h and then slightly reduced at 12 h after IR treatment (Fig. 3*B*). In contrast, ROS levels in cells pretreated with the antioxidant NDGA or GSH were comparable with those of the control group after IR treatment (Fig. 3*C*).

To determine whether IR-induced ROS are associated with cellular senescence, we assessed SA-β-gal activity using NDGA or GSH in irradiated articular chondrocytes. IR-treated cells were positive for the SA-β-gal marker, whereas SA-β-gal was barely detectable in cells pretreated with NDGA or GSH (Fig. 3*D*). However, treatment with ROS inhibitors did not lead to the recovery of senescence-specific morphological changes (Fig. 3*E*) or cell proliferation (Fig. 3*F*). We examined whether senescence-like growth arrest was due to the alterations of p53-pRb pathway. As expected, ROS inhibitors did not reverse the patterns of p53/p21 and p16/pRb pathways changed by IR treatment (Fig. 3*G*), suggesting the involvement of these gene activations in irreversible growth arrest of chondrocytes exposed to IR. These results suggest that ROS generation is necessary for induction of senescence by IR but not maintenance of the senescence phenotype.

Next, we examined the level of total and activated MAPKs in IR-treated chondrocytes, since p38 kinase is induced by various signals and implicated in the onset of cellular senescence (20, 21). As shown in Fig. 4*A*, IR triggered a transient increase in the phosphorylation of ERK and JNK, leading to a peak in their activities at 30 min after treatment. Conversely, phosphorylation of p38 kinase was continuous and lasted up to 12 h after IR treatment. The total cellular MAPK protein levels remained unchanged. We subsequently examined whether IR-induced ROS generation accompanies MAPK activation. For this experiment, chondrocytes were preincubated with NDGA or GSH

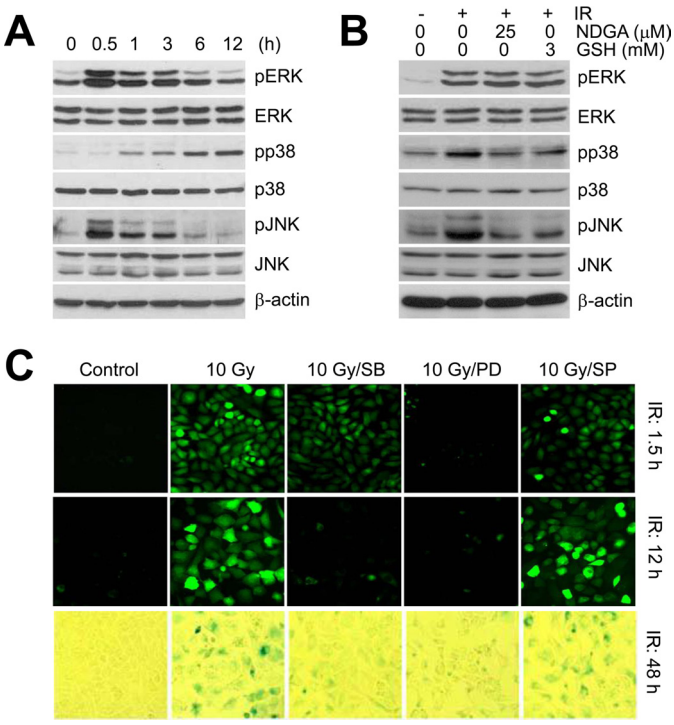

FIGURE 4. **ERK and p38 kinase, but not JNK, act as pivotal mediators of ROS generation during cellular senescence of irradiated articular chondrocytes.** *A*, chondrocytes were treated with 10 Gy of IR and incubated for the indicated periods. Expression and phosphorylation levels of MAPK proteins were determined by Western blotting. β-Actin was used as the loading control. *B*, chondrocytes were left untreated (−) or treated (+) with 10 Gy of IR in the absence or presence of 25 μM NDGA or 3 mM GSH and then incubated for 30 min (for ERK and JNK detection) or 12 h (for p38 detection). Expression and phosphorylation levels of MAPK proteins were determined by Western blotting, with β-actin as the loading control. *C*, chondrocytes were left untreated (control) or treated with 10 Gy of IR in the absence or presence of 20 μM SB202190 (*SB*), 20 μM PD98059 (*PD*), or 20 μM SP600125 (*SP*) and then incubated for 1.5 h (*top*), 12 h (*middle*), or 48 h (*bottom*). Cell staining with DCF-DA to detect ROS was observed under a light microscope (*top* and *middle*), and cellular senescence was evaluated with the SA-β-gal assay (*bottom*). Data are presented as results of a typical experiment (*A* and *B*) or a representative photomicrograph (*C*) from at least four independent experiments.

prior to IR treatment. The compounds did not block ERK activation by IR but inhibited p38 and JNK MAPK activation (Fig. 4*B*), indicating that these processes occur downstream of ROS generation. To establish the feedback linkage between elevation of the intracellular ROS level and MAPK activation in IR-treated articular chondrocytes, cells were preincubated with specific MAPK inhibitors. As shown in Fig. 4*C*, pretreatment of cells with the p38 kinase-specific inhibitor, SB203580, did not affect IR-induced ROS generation at the early time point (90 min; *top*) but led to the complete inhibition of ROS production at a later time point (12 h; *middle*) with concomitant suppression of SA-β-gal activity after IR treatment (48 h; *bottom*). The results support the formation of a ROS-p38 positive feedback loop to sustain down-stream signaling. In contrast, the ERK inhibitor, PD98059, significantly suppressed IR-induced ROS generation at the early and late time points (*top* and *middle*) as well as SA-β-gal activity (*bottom*), indicating that the ERK pathway acts upstream of ROS generation. The JNK-specific inhibitor, SP600125, did not block either ROS generation (*top* and *middle*) or SA-β-gal activity after IR treatment (*bottom*), indicating that this pathway is not associated with IR-induced cellular senescence of articular chondrocytes. Our data collectively suggest that ERK acts as an upstream mediator of ROS generation, leading to effects on p38 kinase activation, with subsequent induction of cellular senescence in primary cultured articular chondrocytes.

p38 Kinase Down-regulates Ubiquitin-independent Post-translational SIRT1 Protein Level in IR-treated Primary Cultured Articular Chondrocytes—Given that the mammalian homolog of Sir2, SIRT1, is involved in various cellular functions and possibly aging (30–39), we examined the expression and activity of this protein. IR treatment with 10 Gy resulted in a time-dependent reduction in the SIRT1 protein level after irradiation and increased acetylation level of histone H3, a major deacetylation substrate of SIRT1 (Fig. 5*A*, *top*). Phosphorylation of p38 was significantly increased up to 24 h and markedly reduced at 48 h after IR. However, NF-κB activation remained unaltered, as determined indirectly using I-κB Western blot analysis (Fig. 5*A*, *top*) and directly with the NF-κB reporter gene assay (Fig. 5*A*, *bottom*). The data suggest that SIRT1 down-regulation is directly or indirectly associated with p38 kinase rather than the NF-κB pathway. To further ascertain whether the degradation of SIRT1 protein is dependent on MAPK activation, we pretreated cells with specific MAPK inhibitors prior to IR. Inhibition of p38 kinase with SB203580 completely rescued IR-induced cleavage of SIRT1 with no alterations in I-κB expression, whereas inhibition of ERK with PD98059 or JNK with SP600125 had no effects on the SIRT1 protein level (Fig. 5*B*). Moreover, stimulation or inhibition of p38 kinase activity with wild-type or dominant negative p38 led to opposite effects on SIRT1 protein level and activity. Specifically, overexpression of wild-type p38 synergistically abolished IR-induced degradation of SIRT1 protein, whereas SIRT1 cleavage was markedly blocked upon direct inhibition of p38 kinase with its dominant negative form. SIRT1 activity was indirectly assayed via detection of the acetylation level of histone H3, which displayed a converse pattern to SIRT1 protein expression (Fig. 5*C*).

To clarify the mechanism of p38 kinase-mediated degradation of SIRT1, we investigated the possible interactions between SIRT1 and p38 kinase. Previous reports show that p38 kinase binds to the docking (D) domain of its substrate, which consists of basic residues and the hydrophobic OA-*X*-OB motif (OA and OB represent Leu, Ile, Met, or Val) (43). Analysis of human SIRT1 amino sequences led to the identification of a binding site located within residues 221–261 containing the L*X*L motif (Fig. 5*D*). It appears that the potential D domain of SIRT1 is vital for the recognition and binding of p38 kinase. SIRT1 was overexpressed in chondrocytes using a retrovirus coding for wild-type SIRT1, and co-immunoprecipitation experiments were performed. Immunoprecipitation of p38 kinase from lysates prepared from these cells led to increased co-precipitation of SIRT1, compared with the control group (Fig. 5*E*, *right*). As expected, IR suppressed complex formation between SIRT1 and p38 kinase, compared with the control group (Fig. 5*E*, *left*). We next examined *in vitro* assay using recombinant GST-p38 kinase fusion protein. Chondrocytes were engineered to overexpress Myc-tagged wild-type SIRT1. Cell lysates were prepared, to which recombinant GST-p38 kinase or GST was added, and the mixture was then analyzed in

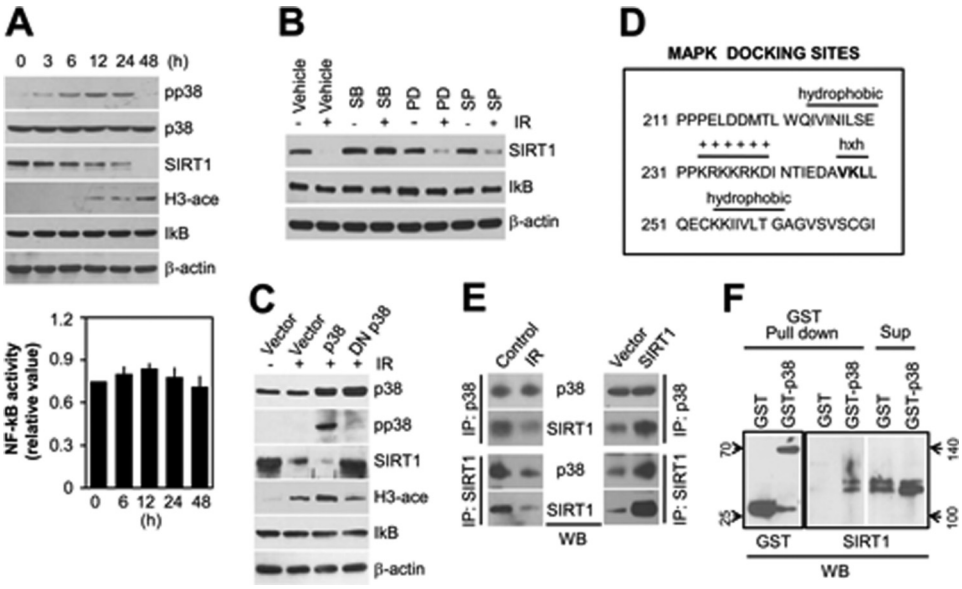

FIGURE 5. **p38 kinase binds to SIRT1 protein *in vivo* and *in vitro* and negatively regulates SIRT1 expression but not NF-κB activity in irradiated primary cultured articular chondrocytes.** *A*, chondrocytes were treated with 10 Gy of IR (*top*) or transfected with NF-κB reporter gene for 24 h and treated with 10 Gy of IR (*bottom*). Cells were then incubated for the indicated periods. Protein levels of p38, SIRT1, and I-κB, phosphorylation of p38, and acetylation of histone H3 were detected by Western blotting (*top*). β-Actin was used as the loading control. NF-κB activity was measured using the reporter gene assay (*bottom*). *B*, chondrocytes were left untreated (−) or treated (+) with 10 Gy of IR in the absence or presence of 20 μM SB202190 (*SB*), 20 μM PD98059 (*PD*), or 20 μM SP600125 (*SP*) and then incubated for 36 h. The expression levels of SIRT1 and I-κB were determined by Western blotting, with β-actin as the loading control. *C*, chondrocytes were transfected with empty vector, p38 expression vector (p38), or dominant negative p38 expression vector (DN p38) for 24 h. Cells were left untreated (−) or treated (+) with 10 Gy of IR and then incubated for an additional 36 h. Protein levels of p38, SIRT1, and I-κB, phosphorylation of p38, and acetylation of histone H3 were detected by Western blotting. β-Actin was used as the loading control. *D*, the SIRT1 sequence is from *Homo sapiens* and shows prospective MAPK docking sites located within residues 211–270. *E*, chondrocytes were left untreated as a control or treated with 10 Gy of IR and incubated for 36 h (*left*) or transfected with empty vector or wild-type SIRT1 expression vector for 24 h (*right*). SIRT1 or p38 was immunoprecipitated (*IP*) from total lysates, and co-precipitation was determined by Western blotting (*WB*). *F*, bacterially expressed recombinant GST-p38 or GST was incubated with cell lysate derived from chondrocytes overexpressing Myc-tagged wild-type SIRT1. Proteins eluted from the bound Sepharose were subjected to Western blot with anti-GST or anti-SIRT1 antibodies. SIRT1 in the supernatant was used as the loading control. Data are presented as results of a typical experiment from at least four independent experiments.

GST pull-down assays. Western blotting for SIRT1 revealed that SIRT1 co-precipitated with GST-p38 kinase but was not detected with GST only (Fig. 5*F*). We also constructed SIRT1-GFP and p38-RFP vectors to determine an accurate binding constant between these two proteins by FRET microscopy. Cells co-expressing SIRT1-GFP and p38-RFP were maintained and imaged before (Fig. 6*A*, *top*) and after (Fig. 6*A*, *bottom*) p38-RFP photobleaching, first with the 488-nm laser line (SIRT1-GFP) and later with the 568-nm laser line (p38-RFP). We chose each speckle in the cytosol or nucleus where SIRT1-GFP and p38-RFP colocalized and measured the fluorescence intensity of SIRT1-GFP, based on the increase of the donor fluorescence after photochemical destruction of the acceptor. p38-RFP was subsequently photobleached by repeated scanning with the 568-nm laser line until no signal was detected. Fluorescent intensity of SIRT1-GFP in the same region before bleaching was clearly increased in the nucleus (Fig. 6*B*, *right*) but not the cytosol (Fig. 6*B*, *left*) compared with prebleach (data not shown). To confirm that FRET signals were not due to fluorophore colocalization, cells were cotransfected with non-fused GFP and non-fused RFP constructs and imaged with the same above process (Fig. 6*C*). Bleaching RFP that colocalized with GFP did not increase GFP fluorescent intensity (Fig. 6*D*) relative to its fluorescence before bleaching (data not shown). Our result shows that SIRT1-GFP fluorescence increased at sites where FRET was occurring, confirming the previous results obtained in co-immunoprecipitation and GST pull-down experiments. Taken together, the data suggest that p38 kinase binds to SIRT1 and regulates both protein expression and activity.

Since the proteasome is responsible for the removal of oxidatively damaged proteins in the cytosol and nucleus during oxidative stress and aging (44), we further examined whether the proteasome-mediated protein degradation pathway is linked with SIRT1 cleavage in primary cultured articular chondrocytes. The SIRT1 protein level was significantly increased in the presence of 26 S proteasome inhibitors (*N*-acetyl-leucyl-leucyl-methioninal and MG132) but not calpain (ALLM) or caspase (Z-VAD-fmk and DEVD-fmk) inhibitors (Fig. 7*A*), suggesting that SIRT1 is degraded via a proteasomal pathway. As expected, the β-catenin protein level, assessed as a positive control, was significantly increased upon inhibition of the 26 S proteasome (Fig. 7, *A* and *B*). Accumulated β-catenin was detected on the gel as a ladder, consistent with ubiquitination (45), but we did not detect electrophoretic mobility shift of SIRT1 following proteasome inhibition (Fig. 7*B*). Since the electrophoretic pattern of SIRT1 suggested non-ubiquitination, we further tested for ubiquitination of SIRT1. Immunoprecipitation and Western blot analysis indicated that β-catenin but not SIRT1 was ubiquitinated in chondrocytes, suggesting that SIRT1 may be degraded by the 26 S proteasome in a ubiquitin-independent manner (Fig. 7*C*). Treatment with the translation inhibitor, cycloheximide, reduced SIRT1 levels, which were further promoted by treatment with IR and blocked by inhibition of the 26 S proteasome with MG132 (Fig. 7*D*). The data confirm that SIRT1 is post-translationally regulated via the proteasome degradation pathway. Post-translational regulation of SIRT1 was additionally supported by our finding that transcript levels were not affected by IR (Fig. 7*E*) or proteasome inhibition (Fig. 7*F*). For characterization of IR-mediated proteasomal degradation of SIRT1, chondrocytes were left untreated or treated with MG132 or ALLnL to inhibit proteasomal activity. IR alone induced suppression of SIRT1 expression compared with the control group, which was completely blocked by both MG132 and ALLnL (Fig. 7*G*).

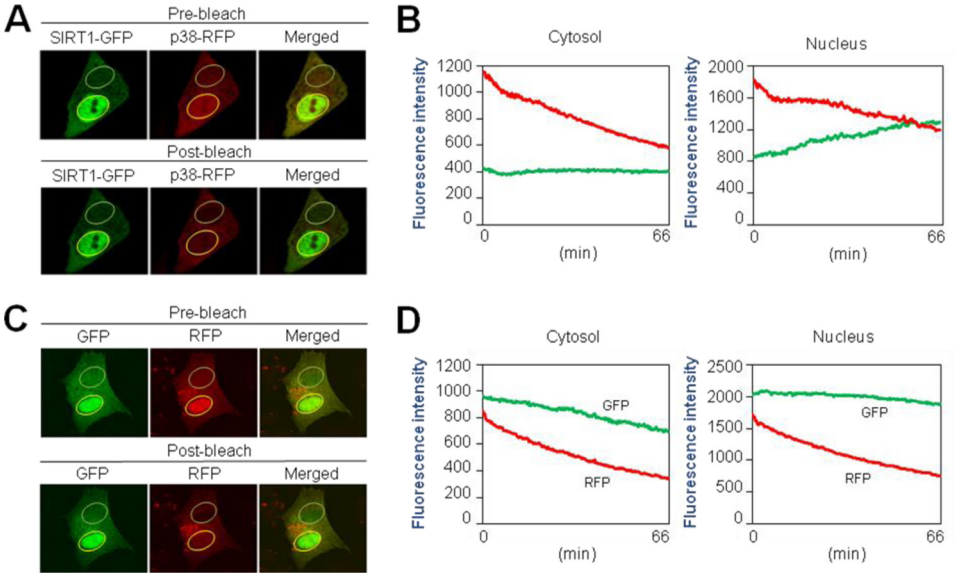

FIGURE 6. **FRET analysis of association between SIRT1 and p38 kinase in primary cultured articular chondrocytes.** *A* and *B*, chondrocytes were cotransfected with SIRT1-GFP and p38-RFP vectors for 48 h. Cells expressing SIRT1-GFP and p38-RFP on coverslips were imaged with confocal fluorescence microscopy, and fluorescence intensity of SIRT1-GFP in the *demarcated regions* (*white circle* for cytosol or *yellow circle* for nucleus) was measured before and after p38-RFP photobleaching (*A*). The *graph* represents the fluorescence intensity of a series (every 20 s) of confocal FRET images after p38-RFP photobleaching in cytosol or nucleus (*B*). *C* and *D*, chondrocytes were cotransfected with non-fused GFP and RFP vectors for 48 h. Cells expressing GFP and RFP on coverslips were imaged with confocal fluorescence microscopy, and fluorescence intensity of GFP in the *demarcated regions* (*white circle* for cytosol or *yellow circle* for nucleus) was measured before and after RFP photobleaching (*C*). The *graph* represents the fluorescence intensity of a series (every 20 s) of confocal FRET images after RFP photobleaching in cytosol or nucleus (*D*). Data are presented as results of a typical experiment from at least four independent experiments.

SIRT1 Acts as a Key Mediator in IR-induced Cellular Senescence of Primary Cultured Articular Chondrocytes—To elucidate the underlying mechanism of SIRT1-mediated regulation of cellular senescence in response to IR, we directly infected chondrocytes with a recombinant retrovirus encoding wild-type SIRT1 or a deacetylase-dead mutant form of dominant-negative SIRT1, SIRT1-HY. Overexpression of wild-type and dominant negative SIRT1 was confirmed by Western blot analysis, and their activities were indirectly assayed by evaluating the acetylation level of histone H3 protein. Whereas control virus-infected cells did not overexpress SIRT1 and displayed a basal level of histone H3 acetylation, IR treatment markedly reduced the SIRT1 protein level and induced high levels of histone H3 acetylation. IR-mediated suppression of SIRT1 activity was recovered in cells expressing wild-type SIRT1 (Fig. 8*A*). However, cells expressing SIRT1-HY alone or in combination with IR displayed inhibited SIRT1 activity, based on the induction of histone H3 acetylation (Fig. 8*A*). Consistent with the data on SIRT1 activity, treatment of cells with IR alone led to increased SA-β-gal activity, which was markedly inhibited by the ectopic expression of wild-type SIRT1 (Fig. 8*B*). However, infection of cells with a retrovirus containing SIRT1-HY alone led to a slight increase in SA-β-gal activity compared with the control group and had no effect on SA-β-gal activity following IR treatment (Fig. 8*B*, *bottom*). The effect of SIRT1 on cellular senescence was additionally evaluated by counting the number of SA-β-gal-positive cells (Fig. 8*C*). We compared the proliferation rates between cells infected with wild-type SIRT1 and SIRT1-HY in response to IR. Compared with IR-treated cells, wild-type SIRT1-infected cells were increased in number following IR. However, the cell number was not restored in cells infected with SIRT1-HY (Fig. 8*D*), consistent with the morphological changes observed in Fig. 8*B* (*top*).

We investigated the biochemical features of senescence using the chemical activator, resveratrol, or the inhibitor, nicotinamide, with a view to further establishing the role of SIRT1 in cellular senescence. Interestingly, no SA-β-gal activity was detected following resveratrol treatment, whereas nicotinamide induced a dramatic increase in the number of SA-β-gal-positive cells, compared with the control group, with no accompanying senescence-specific morphological changes (Fig. 9*A*). This result suggests that the pH 6 β-galactosidase activity detected in nicotinamide-induced senescent cells can be attributed to a rise in the level of the classic lysosomal enzyme. In addition, pretreatment of cells with resveratrol for 1 h prior to IR led to a significant decrease in the appearance of SA-β-gal-positive senescent cells (Fig. 9*B*, *bottom*) with slight morphological changes, similar to the normal phenotype (Fig. 9*B*, *top*). However, nicotinamide did not affect SA-β-gal activity or morphological changes induced by IR (Fig. 9*B*). The pharmacological effects of SIRT1 on cellular senescence were additionally determined by counting the SA-β-gal-positive cells. At 48 h after treatment of cells with resveratrol, the number of SA-β-gal-positive cells decreased to 90% of the initial number evaluated following IR (Fig. 9*C*). Furthermore, a combination of the resveratrol and IR led to a partial increase in cell proliferation, compared with the IR-treated group, but not a combination of nicotinamide and IR (Fig. 9*D*). These results suggest that cellular senescence of articular chondrocytes in response to IR is caused by inhibition of SIRT1 expression and activity.

DISCUSSION

A major aim in the field of radiotherapy is to identify efficient ways to enhance the efficacy of IR in tumors. Apoptosis, a major focus of research, is identified as a crucial biological process in IR-induced cellular dysfunction. Further research is essential to enhance the apoptotic responses of tumor cells. On the other hand, treatment of radiation injuries in normal tissues represents a significant challenge, because many aspects of the pathophysiology of radiation reactions are not completely understood as yet. Recent studies have focused on the association of IR with cellular senescence in both normal and tumor cells (17, 18, 46). In the present investigation, we analyzed the

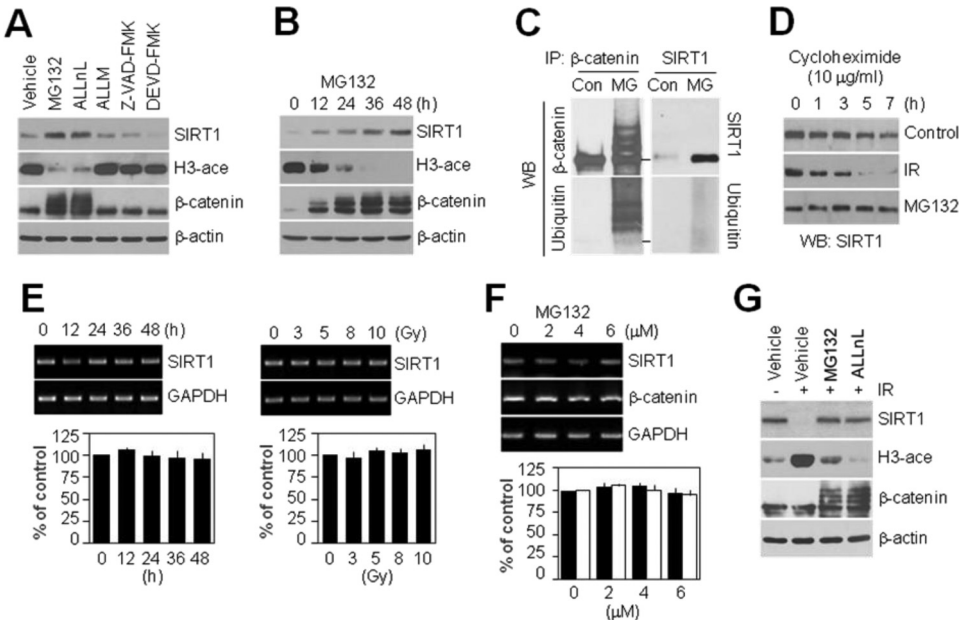

FIGURE 7. **Ubiquitin-independent proteasomal degradation of SIRT1 in primary cultured articular chondrocytes.** *A*, chondrocytes were treated for 24 h with vehicle alone, proteasome inhibitor MG132 (4 μM) or ALLnL (50 μg/ml), the calpain inhibitor ALLM (50 μg/ml), or the caspase inhibitor Z-VAD-FMK (40 μM) or Z-DEVD-FMK (40 μM). Protein levels of SIRT1 and β-catenin and acetylation of histone H3 were determined by Western blotting, with β-actin as the loading control. *B*, chondrocytes were treated with 4 μM MG132 for the indicated periods. Protein levels of SIRT1 and β-catenin and acetylation of histone H3 were determined by Western blotting, with β-actin as the loading control. *C*, chondrocytes were treated with vehicle alone (*Con*) or 4 μM MG132 (*MG*) for 24 h. Total cell lysates were prepared, SIRT1 (*right*) and β-catenin (*left*) were immunoprecipitated (*IP*), and protein ubiquitination was determined by Western blotting (*WB*) using an anti-ubiquitin antibody. *D*, chondrocytes were treated with cycloheximide for the indicated periods in the absence (*Control*) or presence of 10 Gy of IR (*IR*) or 4 μM MG132 (*MG132*). The SIRT1 level was determined by Western blotting. *E* and *F*, chondrocytes were treated with 10 Gy of IR and incubated for the indicated periods (*E*, *left*) with various doses of IR followed by a 48-h incubation (*E*, *right*) or with the indicated concentrations of MG132 for 24 h (*F*). Transcript levels of SIRT1 and β-catenin were determined by conventional PCR (*top*) and quantitative real-time PCR (*bottom*). Glyceraldehyde-3-phosphate dehydrogenase was used as the loading control or internal control. *G*, chondrocytes were treated with vehicle alone, 4 μM MG132, or 50 μg/ml ALLnL for 12 h and then left untreated (−) or acute treated (+) with 10 Gy of IR. At 36 h after irradiation, protein levels of SIRT1 and β-catenin and acetylation of histone H3 were determined by Western blotting. β-Actin was used as the loading control. Data are presented as results of a typical experiment from at least four independent experiments.

effects of radiation on articular chondrocytes and elements of the ROS-related senescence signaling pathway.

IR induced a rapid increase in the ROS level in chondrocytes due to activation of ERK at an early step, as deduced from an ERK inhibition experiment in which the intracellular ROS generated by IR was significantly suppressed (Fig. 4). We have not investigated the mechanism of ROS production by ERK in the present study, but previous reports speculate that ERK phosphorylates integrin or focal adhesion proteins, such as Src/FAK or paxillin, to induce Rac1-associated NADPH oxidase-dependent generation of ROS (47). Furthermore, plasma membrane-bound NADPH oxidase is primarily responsible for intracellular ROS generation in response to ionizing α particles, x-ray, or γ-radiation (48, 49). Therefore, ERK may induce ROS under our experimental conditions, although the cell lines used in individual experiments are different. ROS generation was accompanied by p38 kinase activation in IR-treated chondrocytes, consistent with previous data (23, 50). Interestingly, our data show that p38 kinase activation is a prerequisite for ROS production at the later stage, establishing a positive feedback system for the sustained activation of downstream signaling. Thus, ROS is considered an efficient second intracellular mediator, either downstream of ERK signaling or upstream of p38 kinase, in irradiated chondrocytes. ROS play important roles in physiological processes, including senescence and *in vivo* aging (11–15). Additionally, p38 kinase mediates biological events, including proliferation, differentiation, inflammation, and stress responses (20, 21, 51). Therefore, it is possible that oxidative stress and MAPK activation caused by IR affect chondrocyte function. In fact, IR induced changes in cartilage homeostasis that are relevant to chondrocyte senescence (Fig. 1). However, treatment of cells with the ERK inactivator, PD98059, or p38 kinase inhibitor, SB203580, delayed the onset of senescence via suppression of ROS generation (Fig. 4). Consistent with our findings, other groups reported that high doses of IR efficiently induced premature senescence with specific cell morphology and gene expression in vascular endothelial cells (18). In addition, several cell types, including lung, skin, embryonic fibroblasts, melanocytes, endothelial cells, and retinal pigment epithelial cells, undergo stress-induced premature senescence following exposure to ultraviolet radiation or IR (17). These findings collectively provide evidence supporting the concept that IR-induced ERK and p38 kinase activation are associated with cellular senescence in articular chondrocytes. JNK was activated by IR and decreased by ROS inhibitors in our experiment. However, the IR-induced cellular senescence of articular chondrocytes remained unaffected, indicating no association with the JNK pathway. Several reports demonstrate that chondrocyte senescence promotes cartilage degeneration by decreasing the ability of these cells to maintain and repair articular cartilage tissue (13, 19). Based on the current data, we propose that the destruction of arthritic cartilage is associated with loss of the differentiated phenotype (dedifferentiation), inflammation, and stimulation of matrix metalloproteinases. Our previous reports additionally show that soluble factors, such as Wnt proteins, β-catenin, and IL-1β, induce dedifferentiation of chondrocytes, characterized by suppression of type II collagen expression and onset of type I collagen expression (40, 52). As depicted in Fig. 2, IR led to the down-regulation of mRNA and protein expression of cartilage-specific type II collagen and Sox-9, a major transcription factor that regulates the type II collagen (*COL2A1*) level. Our findings that IR induces cellular senescence and suppression of type II collagen expression in chondrocytes suggest that irradiation may be associated with the progression of cartilage aging and development of OA. This phenomenon is similar to that

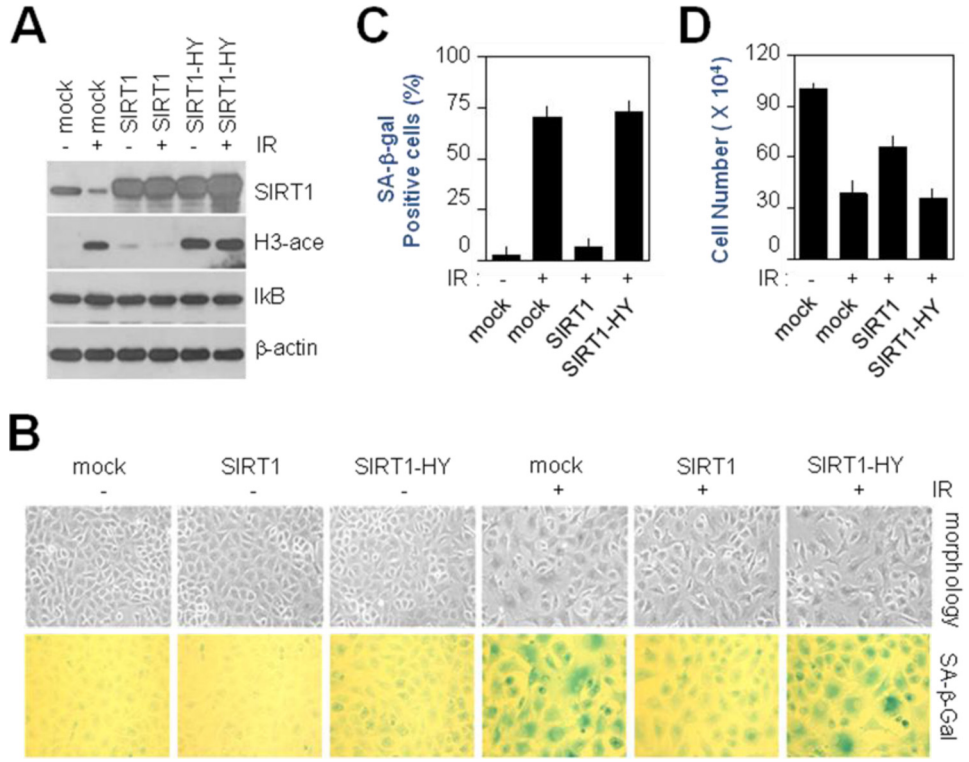

FIGURE 8. **SIRT1 inhibits IR-induced cellular senescence of primary cultured articular chondrocytes with recovery of cell proliferation.** Chondrocytes were infected with control retrovirus (*mock*) or retrovirus containing wild-type (*SIRT1*) or dominant-negative SIRT1 (*SIRT1-HY*) cDNA. Infected cells were cultured in complete medium for 24 h and left untreated (−) or treated (+) with 10 Gy of IR. At 36 h after irradiation, protein levels of SIRT1 and I-κB and acetylation of histone H3 were detected by Western blotting (*A*). β-Actin was used as the loading control. Cell morphology was observed using light microscopy (*B*, *top*), and cellular senescence was evaluated with the SA-β-gal assay (*B*, *bottom*). The *graph* depicts the percentages of SA-β-gal-positive cells counted manually from a total of 200 cells (*C*), and the total cell number was quantified by counting surviving cells using trypan blue solution (*D*). Data are presented as results of a typical experiment (*A*), a representative photomicrograph (*B*), or mean values with S.D. (*C* and *D*) from at least four independent experiments.

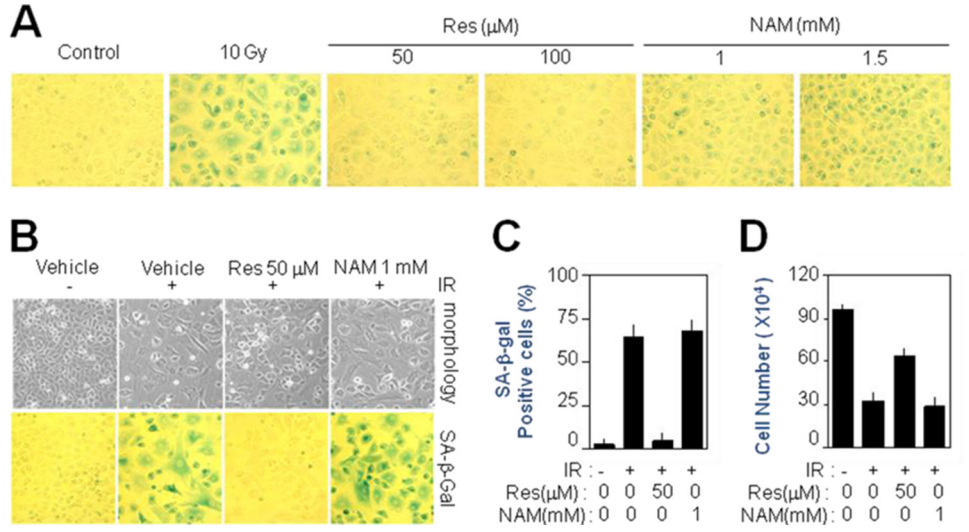

FIGURE 9. **Chemical activation and inhibition of SIRT1 have opposite effects on IR-induced cellular senescence in primary cultured articular chondrocytes.** *A*, chondrocytes were treated with vehicle alone (*Control*), 10 Gy of IR, resveratrol (50 or 100 μM *Res*), or nicotinamide (1 or 1.5 mM *NAM*) and then incubated for 48 h. Cellular senescence was evaluated with the SA-β-gal assay. *B–D*, chondrocytes were treated with vehicle alone, 50 μM resveratrol or 1 mM nicotinamide for 1 h and then left untreated (−) or treated (+) with 10 Gy of IR. At 48 h after irradiation, cell morphology was observed using light microscopy (*B*, *top*), and cellular senescence was evaluated with the SA-β-gal assay (*B*, *bottom*). The *graph* presents the percentages of SA-β-gal-positive cells counted manually from a total of 200 cells (*C*). Total cell number was quantified by counting surviving cells using trypan blue solution (*D*). Data are presented as results of a representative photomicrograph (*A* and *B*) or mean values with S.D. (*C* and *D*) from at least four independent experiments.

observed in endothelial cells, whereby senescence is implicated in the development of age-related diseases, such as atherosclerosis. However, the exact mechanisms underlying chondrocyte senescence remain unclear at present. Our results imply that association of p38 kinase with SIRT1 is a key regulatory mediator in the cellular senescence of articular chondrocytes.

The signaling events downstream of p38 kinase mediating physiological processes in response to various stress signals are a considerable focus of research. In particular, $p16^{INK4A}$, a cyclin-dependent protein kinase inhibitor, and the transcription factor, p53, are two major downstream effectors of p38 kinase in regulating senescence phenotypes (29). Here, we report for the first time that SIRT1, a mammalian NAD^+-dependent deacetylase belonging to class III HDACs, is a downstream effector of p38 kinase and plays an essential role in senescence inhibition in primary cultured articular chondrocytes. As shown in Fig. 5, IR specifically decreases the SIRT1 protein level, with no effects of the transcript level, in a time-dependent manner. This degradation was suppressed by SB203580, a p38 kinase inhibitor, but not ERK and JNK inhibitors or ectopic expression of dominant negative p38 kinase in irradiated chondrocytes. Furthermore, SIRT1 activity was inhibited following p38 kinase activation by ectopic overexpression of wild-type p38. Based on these data, we hypothesize that post-translational down-regulation of SIRT1 in response to IR depends on p38 kinase activity and occurs as a result of direct physical interactions between the two molecules. To further confirm this hypothesis, we investigated the possible interactions between SIRT1 protein and p38 kinase. Co-immunoprecipitation experiments revealed that p38 kinase normally bound to SIRT1 protein in chondrocytes, although this interaction was significantly decreased by IR and increased upon ectopic overexpression of SIRT1,

compared with the control group. We also carried out extensive quantitative analysis of FRET data to show interaction of these two proteins. The data showing their direct interaction in the nucleus suggest that the nuclear localization is important for SIRT1 function in regulation of cellular senescence of chondrocytes in response to IR (Fig. 6). In addition, MAPKs interact specifically with numerous proteins during the signaling cascade via highly specific docking sites (53). Chang *et al.* (54) reported that the crystallographic structure of p38 kinase contains a common docking domain, which interacts with a conserved motif (D domain) on substrate molecules. D domain forms a modular structure, consisting of a basic region and a cluster of positively charged residues, designated the L*X*L motif, surrounded by a hydrophobic region. Our sequence analysis disclosed the presence of a potential D domain in SIRT1 containing the L*X*L motif (^{247}VKL^{249}) and a hydrophobic pocket in its HDAC domain. These results collectively provide evidence for SIRT1 protein degradation via IR-induced p38 kinase activation. In relation to other known MAPKs, JNK2 is linked with SIRT1 protein stability, either directly or indirectly via phosphorylation at serine 27 in human cells (55). However, under our experimental conditions, JNK2 did not appear to be involved in SIRT1 regulation in primary cultured articular chondrocytes, because we detected no changes in SIRT1 protein levels before and after treatment with the JNK inhibitor, SP600125, in Western blot analyses. Moreover, the JNK pathway was not involved in IR-induced cellular senescence of chondrocytes, coincident with its lack of association with SIRT1.

As indicated above, the SIRT1 protein is down-regulated by binding with activated p38 kinase in response to IR. Accordingly, we examined the regulatory mechanisms of SIRT1 degradation and the role of the protein in IR-induced cellular senescence of articular chondrocytes. We conclude that SIRT1 is post-translationally regulated by p38 kinase in articular chondrocytes, since IR treatment and proteasome inhibition had no effects on the transcript levels. This theory is supported by data on the SIRT1 protein half-life, which is reduced in the presence of the translational inhibitor, cycloheximide, and increased by the proteasome inhibitor, MG132 (Fig. 7). It appears that the decrease in SIRT1 protein in articular chondrocytes is not attributable to transcription levels but reflects protein stability. Furthermore, this is the first study to report that SIRT1 is degraded via a proteasomal pathway in normal articular chondrocytes. We further demonstrate complete blockage of IR-induced SIRT1 degradation by MG132 or ALLnL, providing evidence of proteasomal cleavage. Another interesting feature of the SIRT1 protein is the presence of the PEST sequence at residues 525–550 and 667–697. The PEST sequence acts as a signal peptide for protein degradation, and this cleavage is possibly mediated via the proteasome or calpain (56, 57). The presence of two PEST regions in SIRT1 is correlated with rapid degradation of the protein by 26 S proteasome protease. In typical proteasomal protein degradation, the rate-limiting step is the recruitment of the ubiquitin-protein isopeptide ligase (E3), which conjugates a polyubiquitin to the substrate (58). However, we did not observe clear evidence of Sirt1 ubiquitination in articular chondrocytes, suggesting that the protein may be degraded via the 26 S proteasome in a ubiquitination-independent manner. Earlier studies, including a report by our group, show that several proteins undergo ubiquitin-independent proteasome-dependent cleavage (59). Accordingly, we suggest that SIRT1 is recognized by the 26 S proteasome and may be cleaved post-translationally in a ubiquitin-independent manner via phosphorylation by p38 kinase activation. However, the mechanism underlying phosphorylation of SIRT1 requires further examination. Recent reports show that SIRT1 is involved in a number of cellular processes, including longevity and gene silencing, via interaction with p53, FOXO, PPAR-γ, and Ku 70 (30, 32–35, 37, 39). SIRT1 inhibition by sirtinol induces premature senescence-like growth arrest in human cancer cells and mouse fibroblast cells (60). Consistent with previous data, SIRT1 inhibition by IR induced the cellular senescence phenotype in articular chondrocytes, and elevation of the protein level or activity prevented cellular senescence promoted by IR. These effects were similar between direct SIRT1 gene applications and indirect pharmacological methods regulating SIRT1 activity, as evident from the representative markers for cellular senescence, SA-β-gal activity, cell growth arrest, and morphology (Figs. 8 and 9). However, the molecular regulatory mechanisms underlying cellular senescence by SIRT1 in articular chondrocytes remain to be clarified. One theory is that SIRT1 modulates cellular senescence by antagonizing p53 activity in articular chondrocytes. As specified above, p53 is a major downstream effector of p38, and its acetylation is reported to induce cellular senescence. Moreover, previous investigations report that SIRT1 inactivates the transcriptional activity of p53 via deacetylation (32, 33). The findings that IR induces down-regulation of SIRT1 activity followed by promotion of cellular senescence, as well as the reversible effects of elevation or activation of SIRT1, are consistent with regulatory phenomena of p53 activity and senescence. Based on these results, we propose that SIRT1 regulates cellular senescence through modulation of p53 activity (Fig. 10).

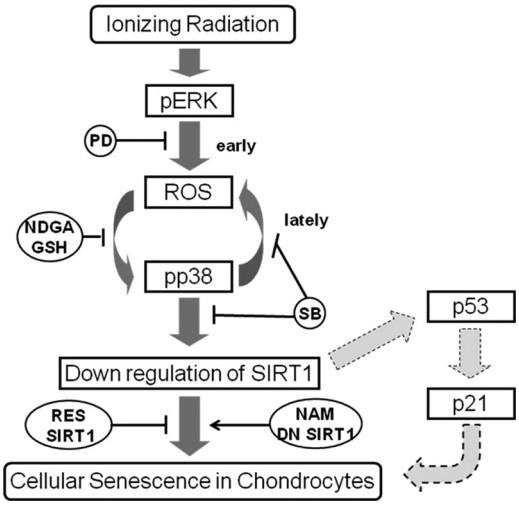

FIGURE 10. **Schematic summary of a signaling pathway underlying IR-induced cellular senescence of primary cultured articular chondrocytes.** *pERK*, phospho-ERK; *PD*, PD98059; *SB*, SB202190; *RES*, resveratrol; *NAM*, nicotinamide.

In summary, induction of cellular senescence is a common response of normal cells to a DNA-damaging agent, which may

contribute to IR-induced normal tissue injury. Regulation of the SIRT1 level in response to IR is an important event for controlling cellular senescence. Physical interactions between p38 kinase and SIRT1 led to down-regulation of the SIRT1 protein level in IR-treated articular chondrocytes. Inhibition of senescence using SIRT1 or specific inhibitors of the p38 kinase pathway appears to be effective therapy for IR-induced normal tissue damage and may be applied in the treatment of OA. Further studies are required to identify other molecular mechanisms promoting positive effects in maintaining healthy normal articular chondrocytes following IR exposure.

REFERENCES

1. Hristov, B., Shokek, O., and Frassica, D. A. (2007) *J. Natl. Compr. Canc. Netw.* **5,** 456–466
2. Patel, S., and DeLaney, T. F. (2008) *Cancer Control* **15,** 21–37
3. Goldwein, J. W. (1991) *Clin. Orthop. Relat. Res.* **262,** 101–107
4. Robertson, W. W., Jr., Butler, M. S., D'Angio, G. J., and Rate, W. R. (1991) *J. Pediatr. Orthop.* **11,** 284–287
5. Kroll, S. S., Woo, S. Y., Santin, A., Zietz, H., Ried, H. L., Jaffe, N., and Larson, D. L. (1994) *Ann. Surg. Oncol.* **1,** 473–479
6. Damron, T. A., Mathur, S., Horton, J. A., Strauss, J., Margulies, B., Grant, W., Farnum, C. E., and Spadaro, J. A. (2004) *J. Histochem. Cytochem.* **52,** 157–167
7. Pateder, D. B., Sheu, T. J., O'Keefe, R. J., Puzas, J. E., Schwarz, E. M., Constine, L. S., Okunieff, P., and Rosier, R. N. (2002) *Radiat. Res.* **157,** 62–68
8. Damron, T. A., Margulies, B. S., Strauss, J. A., O'Hara, K., Spadaro, J. A., and Farnum, C. E. (2003) *J. Bone Joint Surg. Am.* **85,** 1302–1313
9. Matsumura, T., Zerrudo, Z., and Hayflick, L. (1979) *J. Gerontol.* **34,** 328–334
10. Dimri, G. P., Lee, X., Basile, G., Acosta, M., Scott, G., Roskelley, C., Medrano, E. E., Linskens, M., Rubelj, I., and Pereira-Smith, O. (1995) *Proc. Natl. Acad. Sci. U.S.A.* **92,** 9363–9367
11. Serrano, M., Lin, A. W., McCurrach, M. E., Beach, D., and Lowe, S. W. (1997) *Cell* **88,** 593–602
12. Zhu, J., Woods, D., McMahon, M., and Bishop, J. M. (1998) *Genes Dev.* **12,** 2997–3007
13. Yudoh, K., Nguyen, T., Nakamura, H., Hongo-Masuko, K., Kato, T., and Nishioka, K. (2005) *Arthritis Res. Ther.* **7,** R380–391
14. Sedelnikova, O. A., Horikawa, I., Zimonjic, D. B., Popescu, N. C., Bonner, W. M., and Barrett, J. C. (2004) *Nat. Cell Biol.* **6,** 168–170
15. Chen, J. H., Ozanne, S. E., and Hales, C. N. (2005) *DNA Repair (Amst.)* **4,** 1140–1148
16. Kanaar, R., Hoeijmakers, J. H., and van Gent, D. C. (1998) *Trends Cell Biol.* **8,** 483–489
17. Oh, C. W., Bump, E. A., Kim, J. S., Janigro, D., and Mayberg, M. R. (2001) *Radiat. Res.* **156,** 232–240
18. Igarashi, K., Sakimoto, I., Kataoka, K., Ohta, K., and Miura, M. (2007) *Exp. Cell Res.* **313,** 3326–3336
19. Aigner, T., Kurz, B., Fukui, N., and Sandell, L. (2002) *Curr. Opin. Rheumatol.* **14,** 578–584
20. Iordanov, M., Bender, K., Ade, T., Schmid, W., Sachsenmaier, C., Engel, K., Gaestel, M., Rahmsdorf, H. J., and Herrlich, P. (1997) *EMBO J.* **16,** 1009–1022
21. Nebreda, A. R., and Porras, A. (2000) *Trends Biochem. Sci.* **25,** 257–260
22. Wang, W., Chen, J. X., Liao, R., Deng, Q., Zhou, J. J., Huang, S., and Sun, P. (2002) *Mol. Cell. Biol.* **22,** 3389–3403
23. Jung, M. S., Jin, D. H., Chae, H. D., Kang, S., Kim, S. C., Bang, Y. J., Choi, T. S., Choi, K. S., and Shin, D. Y. (2004) *J. Biol. Chem.* **279,** 17765–17771
24. Haq, R., Brenton, J. D., Takahashi, M., Finan, D., Finkielsztein, A., Damaraju, S., Rottapel, R., and Zanke, B. (2002) *Cancer Res.* **62,** 5076–5082
25. Xu, H. J. (1997) *Adv. Pharmacol.* **40,** 369–397
26. Taher, M. M., Hershey, C. M., Oakley, J. D., and Valerie, K. (2000) *Photochem. Photobiol.* **71,** 455–459
27. Wang, X., McGowan, C. H., Zhao, M., He, L., Downey, J. S., Fearns, C., Wang, Y., Huang, S., and Han, J. (2000) *Mol. Cell. Biol.* **20,** 4543–4552
28. Lee, Y. J., Soh, J. W., Dean, N. M., Cho, C. K., Kim, T. H., Lee, S. J., and Lee, Y. S. (2002) *Cell Growth Differ.* **13,** 237–246
29. Han, J., and Sun, P. (2007) *Trends Biochem. Sci.* **32,** 364–371
30. Hekimi, S., and Guarente, L. (2003) *Science* **299,** 1351–1354
31. Vaquero, A., Scher, M., Lee, D., Erdjument-Bromage, H., Tempst, P., and Reinberg, D. (2004) *Mol. Cell* **16,** 93–105
32. Luo, J., Nikolaev, A. Y., Imai, S., Chen, D., Su, F., Shiloh, A., Guarente, L., and Gu, W. (2001) *Cell* **107,** 137–148
33. Vaziri, H., Dessain, S. K., Ng Eaton, E., Imai, S. I., Frye, R. A., Pandita, T. K., Guarente, L., and Weinberg, R. A. (2001) *Cell* **107,** 149–159
34. Brunet, A., Sweeney, L. B., Sturgill, J. F., Chua, K. F., Greer, P. L., Lin, Y., Tran, H., Ross, S. E., Mostoslavsky, R., Cohen, H. Y., Hu, L. S., Cheng, H. L., Jedrychowski, M. P., Gygi, S. P., Sinclair, D. A., Alt, F. W., and Greenberg, M. E. (2004) *Science* **303,** 2011–2015
35. Motta, M. C., Divecha, N., Lemieux, M., Kamel, C., Chen, D., Gu, W., Bultsma, Y., McBurney, M., and Guarente, L. (2004) *Cell* **116,** 551–563
36. Yeung, F., Hoberg, J. E., Ramsey, C. S., Keller, M. D., Jones, D. R., Frye, R. A., and Mayo, M. W. (2004) *EMBO J.* **23,** 2369–2380
37. Picard, F., Kurtev, M., Chung, N., Topark-Ngarm, A., Senawong, T., Machado De Oliveira, R., Leid, M., McBurney, M. W., and Guarente, L. (2004) *Nature* **429,** 771–776
38. Wang, C., Chen, L., Hou, X., Li, Z., Kabra, N., Ma, Y., Nemoto, S., Finkel, T., Gu, W., Cress, W. D., and Chen, J. (2006) *Nat. Cell Biol.* **8,** 1025–1031
39. Cohen, H. Y., Miller, C., Bitterman, K. J., Wall, N. R., Hekking, B., Kessler, B., Howitz, K. T., Gorospe, M., de Cabo, R., and Sinclair, D. A. (2004) *Science* **305,** 390–392
40. Hwang, S. G., Yu, S. S., Poo, H., and Chun, J. S. (2005) *J. Biol. Chem.* **280,** 29780–29787
41. Clutton, S. M., Townsend, K. M., Walker, C., Ansell, J. D., and Wright, E. G. (1996) *Carcinogenesis* **17,** 1633–1639
42. Morales, A., Miranda, M., Sánchez-Reyes, A., Biete, A., and Fernández-Checa, J. C. (1998) *Int. J. Radiat. Oncol. Biol. Phys.* **42,** 191–203
43. Bardwell, L., and Shah, K. (2006) *Methods* **40,** 213–223
44. Breusing, N., and Grune, T. (2008) *Biol. Chem.* **389,** 203–209
45. Aberle, H., Bauer, A., Stappert, J., Kispert, A., and Kemler, R. (1997) *EMBO J.* **16,** 3797–3804
46. Podtcheko, A., Namba, H., Saenko, V., Ohtsuru, A., Starenki, D., Meirmanov, S., Polona, I., Rogounovitch, T., and Yamashita, S. (2005) *Thyroid* **15,** 306–313
47. Honoré, S., Kovacic, H., Pichard, V., Briand, C., and Rognoni, J. B. (2003) *Exp. Cell Res.* **285,** 59–71
48. Narayanan, P. K., Goodwin, E. H., and Lehnert, B. E. (1997) *Cancer Res.* **57,** 3963–3971
49. Tateishi, Y., Sasabe, E., Ueta, E., and Yamamoto, T. (2008) *Biochem. Biophys. Res. Commun.* **366,** 301–307
50. Guyton, K. Z., Liu, Y., Gorospe, M., Xu, Q., and Holbrook, N. J. (1996) *J. Biol. Chem.* **271,** 4138–4142
51. Ono, K., and Han, J. (2000) *Cell. Signal.* **12,** 1–13
52. Hwang, S. G., Ryu, J. H., Kim, I. C., Jho, E. H., Jung, H. C., Kim, K., Kim, S. J., and Chun, J. S. (2004) *J. Biol. Chem.* **279,** 26597–26604
53. Sharrocks, A. D., Yang, S. H., and Galanis, A. (2000) *Trends Biochem. Sci.* **25,** 448–453
54. Chang, C. I., Xu, B. E., Akella, R., Cobb, M. H., and Goldsmith, E. J. (2002) *Mol. Cell* **9,** 1241–1249
55. Ford, J., Ahmed, S., Allison, S., Jiang, M., and Milner, J. (2008) *Cell Cycle* **7,** 3091–3097
56. Rogers, S., Wells, R., and Rechsteiner, M. (1986) *Science* **234,** 364–368
57. Reverte, C. G., Ahearn, M. D., and Hake, L. E. (2001) *Dev. Biol.* **231,** 447–458
58. Dantuma, N. P., and Masucci, M. G. (2002) *FEBS Lett.* **529,** 22–26
59. Hwang, S. G., Yu, S. S., Ryu, J. H., Jeon, H. B., Yoo, Y. J., Eom, S. H., and Chun, J. S. (2005) *J. Biol. Chem.* **280,** 12758–12765
60. Ota, H., Akishita, M., Eto, M., Iijima, K., Kaneki, M., and Ouchi, Y. (2007) *J. Mol. Cell. Cardiol.* **43,** 571–579